

# Mechanism for BCC to HCP Transformation: Generalization of the Burgers Model

S.G. Srinivasan,<sup>\*</sup> D.M. Hatch,<sup>†</sup> H.T. Stokes,<sup>‡</sup> A. Saxena, R.C. Albers, and T. Lookman  
*Theoretical Division, Los Alamos National Laboratory, Los Alamos, New Mexico 87545.*

(Dated: March 22, 2022)

## Abstract

Many structural transformations involve a group-nonsubgroup relationship between the initial and transformed phases, and hence are beyond the purview of conventional Landau theory. We utilize a systematic and robust methodology to describe such reconstructive martensitic transformations by coupling group-theoretical arguments to first-principles calculations. In this context we (i) use a symmetry-based algorithm to enumerate transformation paths, (ii) evaluate the energy barriers along these transformation paths using all-electron first principles calculations, (iii) deduce the full set of primary and secondary order parameters for each path to establish the appropriate Ginzburg-Landau free-energy functionals, and (iv) for each path, identify special points of the primary order parameter, as a function of local distortions, corresponding to the end product phase. We apply this method to the study of a pressure driven body-centered cubic (bcc) to hexagonal close-packed (hcp) transformation in titanium. We find a generalization of the Burgers mechanism, and also find that there is no energy barrier to this transformation. In fact, surprisingly, we also find a region of volumes in which the intermediate path becomes more stable than either of the end-points (bcc or hcp). We therefore predict a new orthorhombic phase for Ti between 51 and 62 GPa.

PACS numbers: 81.30.Kf, 64.70.Kb, 05.70.Fh

## I. INTRODUCTION

Polymorphism, *i.e.*, the changing of a solid from one crystal structure variant to another, is abundant in both nature and in engineering technologies. The body-centered-cubic (bcc) to hexagonal-close-packed (hcp) structural transition discussed in this paper is a well-known example. For instance, iron undergoes this transformation at very high pressure ( $\sim 13$  GPa) in the core of the earth as well as under shock conditions in diamond anvil experiments<sup>1</sup>. Certain seismic activity has been attributed to strain generated during this phase change. Toughness and ductility in Ti and Zr, which undergo this transformation at high temperature, are two important issues for the aerospace industry. In addition to these three elements, the bcc-hcp transformation is found in eighteen other elements, such as Ba, Mg, Hf, Sc, Tl, and Y, and their alloys.

Polymorphic diffusionless transformations have been broadly classified as either displacive or reconstructive. In the displacive transformation there is no change in the first coordination of the atoms in both the initial and the transformed phases. The energy differences between these two phases arise from changes in the secondary coordination. In terms of crystal symmetry, the transformed phase is a slightly altered derivative crystal structure, a subgroup, of the initial phase. In the reconstructive transformation, bonds are broken and then reformed to suit the transformed phase. Consequently, there is a change in the primary coordination. The transformed phase is no longer a slightly altered structure of the initial phase; it is not a subgroup structure of the parent phase (or, vice-versa). In diffusionless polymorphic transformations, individual atoms execute ordered and correlated motions, and significant transformational strains may also develop in this process. These are the so-called martensitic transformations (MT).

The study of MT has a long and rich history. Early attempts by metallurgists to understand both displacive and reconstructive MT's ignored the need to maintain coherency between the initial and transformed structures as the transformation progressed. That neglect hindered the development of an atomistic understanding of the transformation mechanism in terms of simple shears of the crystal cell coupled with local atom readjustments (shuffles). Thus, martensite theories often chose the phenomenological route of geometrically relating the initial and transformed phases, ignoring the atomistic pathways and microscopic mechanisms driving the transformation. A well-known phenomenological theory of Wechsler,

Lieberman and Read successfully demonstrated that a MT can be understood at this level in terms of three basic deformations<sup>2,3,4</sup>. Nevertheless, within the above mentioned phenomenological approach, microscopic mechanisms were identified for many reconstructive transformations, purely from the orientational relationships between the initial and transformed phases. In Table I we give examples of several common mechanisms.

More recently, physicists have successfully used the phenomenological Landau theory to model displacive MT for a nearly continuous (*i.e.*, weakly first order) transformation. Because the displacive MT is nearly continuous, the invariant free-energy (invariant under the symmetry group of the initial phase) defines an order parameter (OP) onset. The Landau philosophy has recently been extended to a phenomenological theory of reconstructive phase transitions by expressing the OP function as a density-wave function of the atomic displacements<sup>10</sup>. Note that an effective *one-dimensional* Ginzburg-Landau model for Ti and Zr<sup>11</sup> has been combined previously with electronic structure calculations<sup>12</sup>. The bcc-hcp transition in titanium occurs around 1150 K. However, here we attempt to model this transition at  $T = 0$  by varying the pressure: bcc is the high-pressure phase and the hcp the low-pressure phase. The bcc-hcp transformation pathways and mechanisms elaborated below are generic to the bcc-hcp transition in a wide variety of elements and alloys. In effect, the temperature variation in titanium is mimicked by pressure variation at  $T = 0$  capturing the essential pathways of the transition, specifically the intermediate orthorhombic phase. As discussed below, we surprisingly find that one of the pathways becomes more stable than either the bcc or hcp end-points in Ti for a range of volumes. We therefore predict a new orthorhombic phase transformation in Ti at low temperature. This paper is organized as follows. In the next section we introduce the concept of a common subgroup. In Sec. III we enumerate the various symmetry based pathways for the bcc-hcp phase transition. In Sec. IV we describe the first-principles calculations performed here. Section V gives an overview of the Landau free-energy fitting. Results and discussions are contained in Sec. VI.

## II. THE COMMON SUBGROUP PARADIGM AND TRANSFORMATION PATHS

The bcc-hcp transformation in Ti considered here is a reconstructive martensitic transformation. There is no group-subgroup relationship between the space groups of the bcc

( $Im\bar{3}m$ ) and hcp ( $P6_3/mmc$ ) phases participating in the transformation. Burgers<sup>6</sup> originally proposed the orientational relationship between the bcc and hcp phases in Zr: the basal  $\{0001\}_{\text{hcp}}$  plane is parallel to a  $\{110\}_{\text{bcc}}$  plane, and a  $\langle 11\bar{2}0 \rangle$  close-packed direction in the hcp basal plane is parallel to a cubic  $\langle 111 \rangle$  direction. A combination of three lattice distortions can lead to this transformation<sup>13,14,15</sup>: (i) a shuffle displacement of the  $\{110\}_{\text{bcc}}$  planes in the  $\langle 1\bar{1}0 \rangle$  directions. A displacement amplitude of  $\frac{\sqrt{2}}{12}$  times the bcc lattice constant leads to the exact hcp stacking sequence. (ii) A shear such as  $(1\bar{1}2) [\bar{1}11]$  and  $(\bar{1}12)[1\bar{1}1]$  to squeeze the bcc octahedron into a regular hcp one. The angle of the hcp face in the basal plane changes from  $70.53^\circ$  to  $60^\circ$ . The Burgers mechanism was painstakingly determined by studying the orientational relationships between bcc and hcp phases. It is understood in terms of the three parameters, shuffle, shear, and volume dilatation.

In this paper we present a more general and robust approach for identifying reconstructive transition mechanisms based on crystallographic group theory. It is equally applicable to bcc-hcp MT's in other elements, or for other reconstructive MT's such as the transitions fcc-hcp, hcp- $\omega$ , etc. The distortion of a crystal can clearly destroy some of its symmetry elements and force it into one of its lower symmetry subgroups. As atoms move from one structure toward another, symmetry is lowered as the atoms leave their high symmetry locations. We assume initially that this lower symmetry is maintained until at some suitable, large displacement it is able to lock-in to the symmetry of the transformed phase. We thus hypothesize that the reconstructive transformations proceed via a subgroup common to both the initial and transformed phases. This requires the atoms to sensibly map from the initial structure onto the subgroup, and then onto the final structure. By imposing some restrictions on cell size changes the number of available transformational paths equals a finite number of maximal subgroups<sup>16</sup>, with compatible atomic mappings, common to both the initial and the transformed structures. We can then look for even lower symmetry structures along the path by testing stability within the maximal subgroup phase. The actual path chosen is ultimately decided by the nature of the interatomic interactions in the material. Coupling the symmetry with interatomic force calculations gives us a general, systematic, and robust recipe to explore the different pathways, and identify the minimum energy path(s) among them. This method is amenable to automation by computer and can quickly search for transformational paths between any two of the 230 crystallographic space-groups.

We illustrate an application of our procedure by coupling the full potential linear

augmented-plane-wave (FLAPW) method to crystal symmetry information in order to enumerate all possible paths for the bcc-hcp transformation in titanium. Based just on symmetry conditions, we initially obtain six possible mechanisms for the bcc-hcp transformation in titanium. Of these six, one is energetically favored and is similar to the Burgers mechanism. Our mechanism adds an effective interplanar variance to the three parameters used in the original Burgers mechanism. In this work, we extend the Landau philosophy to reconstructive MT's by including local site symmetry information. Our procedure is distinct from that given in Toledano et al.<sup>10</sup> in that we do not assume a transcendental stationary density-wave description but instead structure our approach on common subgroup symmetry aspects and a more conventional Landau position-dependent OP. However, we do use specific intracell correspondences of atoms in the two structures, which is not contained in the conventional Landau procedure, and look for the onset of new symmetry elements at the end product phase. These features are in common with the description given by Toledano et al.<sup>10</sup> We fit a Landau free-energy functional over the multi-component OPs in this transition. The free-energy functional is fitted using the first principles energy values obtained for the most plausible transformation mechanism.

The bcc-hcp transition in titanium occurs around 1150 K. Here we attempt to model this transition at  $T = 0$  by varying the pressure: bcc is the high-pressure phase and hcp the low-pressure phase. In this sense our modeling cannot be considered as realistic in capturing the (temperature induced) transition in titanium. However, two new high-pressure phases of titanium have been observed recently, namely  $\gamma$ -Ti which is a distorted hcp structure at 128 GPa<sup>17,18</sup> and  $\delta$ -Ti which is a distorted bcc structure at 140 GPa<sup>18</sup>. Interestingly, both of these structures are orthorhombic with the space group  $Cmcm$  and the lattice deformations can be interpreted within the framework of our generalized Burgers mechanism. We also predict a new orthorhombic phase transformation between 51 and 62 GPa at zero temperature. In this context our modeling is directly relevant to pressure induced transitions in titanium. In addition, the bcc-hcp transformation pathways and mechanisms elaborated below are representative of the bcc-hcp transition in a wide variety of elements (e.g. Zr, Hf) and alloys. In effect, the temperature variation in titanium is mimicked by pressure variation at  $T = 0$  capturing the essential pathways of the transition, specifically the intermediate orthorhombic phase.

### III. CRYSTAL SYMMETRY BASED ALGORITHM TO DETERMINE THE MECHANISM FOR THE BCC-HCP TRANSFORMATION

Methods based solely on orientational relationships between the initial and transformed phases force one to “guess” the transformational mechanism. Even symmetry based information coupled with atomic site correspondence does not unequivocally reveal the transformational mechanism. Our approach here is to use “physics” insight (interatomic forces based on first-principles or some other suitable semi-empirical method) to interrogate the various common subgroup based symmetry pathways to determine plausible paths based on their relative energies. We expect that the minimum energy path, under the transformational conditions, will be favored, and we initially consider maximal symmetry pathways. Overall, such an approach reduces the systematic search of paths to a smaller number. In this process, we can also identify the primary and secondary order-parameters, the Ginzburg-Landau invariants, and declare the special OP lock-in values corresponding to the transformed phase.

To describe a reconstructive phase transition, one must address two important questions: (1) How are the atoms mapped from one structure onto the other? (2) What distortional pathway do the atoms take between these two structures? The mapping question deals with how the two structures are related. The path question is more difficult. It deals with actual atomic displacements and strains that occur during the phase transition. In an earlier paper we presented a systematic procedure for obtaining possible mappings (paths) for a reconstructive phase transition in two dimensions (2D)<sup>19</sup>, namely the square lattice to triangular lattice transition, based essentially on symmetry considerations. In that treatment, it was assumed the pathway between the two structures proceeded by means of an intermediate common unstable structure (either an oblique lattice or a centered rectangular lattice) with definite space-group symmetry  $G$ . Note that the square→triangle transformation is a 2D analog of the bcc-hcp transformation. If we are considering a reconstructive phase transition from a structure with space-group symmetry  $G_1$  to a structure with space-group symmetry  $G_2$ , then our description is actually a two-step process,  $G_1 \rightarrow G \rightarrow G_2$ , where  $G$  is a subgroup of  $G_1$  and also a subgroup of  $G_2$  so that each step,  $G_1 \rightarrow G$  and  $G \rightarrow G_2$ , is a transition with a group-subgroup relationship.

The first question stated above is related to the mapping of atoms through a subgroup and was systematically addressed by a four step algorithm<sup>19</sup>. We describe this algorithm

using the bcc-hcp transformation as an example. However, it is general and applies to other reconstructive transformations. The tables of Stokes and Hatch<sup>16</sup> were used to obtain the needed information at each of the following four steps.

*Step-1:* Find the subgroups common to both the initial (bcc) and transformed (hcp) phases. To begin, it is convenient to look at common subgroups arising from distortions corresponding to  $\mathbf{k}$  points of symmetry. We find seventeen subgroups which are subgroups of both the hcp and bcc phase.

*Step-2:* Subgroups arise from microscopic displacements and/or macroscopic strains. Strain cannot be the primary OP since the bcc-hcp transition involves primitive cell doubling. Shuffle is our primary OP and the induced representation formalism is used to determine which irreducible-representations (IR's) allow microscopic atomic  $x, y, z$  displacements from each parent group into the subgroups. Only fifteen subgroups are consistent with this requirement.

*Step-3:* Atoms are at the 2(a) and 2(c) Wyckoff positions in bcc and hcp respectively. Subgroups that relate bcc and hcp phases must have compatible Wyckoff positions. Each acceptable subgroup is connected to a specific IR and mode form (OP direction). Thus, there is a precise atom to atom identification throughout the transformational path. This ensures consistency as the Wyckoff position changes (or splits) as the transformation moves from bcc to hcp. After applying this constraint, we are left with fourteen subgroups corresponding to fifty-eight possible mechanisms.

*Step-4:* We determine a specific (correlated) displacement mechanism for each IR and subgroup. All possible mechanisms for the bcc-hcp transformation based on this algorithm are given in Table II. Of these, we restrict our attention to the most simple mechanisms such as a maximum cell size change of two and a P1 or P2 (one parameter) OP direction. As can be seen from Table II, these two restrictions yield three mechanisms;  $H_4^- 63(\text{P2},2)$ ,  $N_2^- 63(\text{P1},2)$ , and  $N_4^- 63(\text{P1},2)$ . This notation gives the IR, the identifying number of the subgroup, the order parameter direction, and the cell size change. The atomic displacements for these mechanisms are shown in Fig. 1. Note that the space group symmetry of the common subgroup is the same and the atoms go into the Wyckoff  $c$  positions for each of the 3 paths.

The labeling of representations is that of Miller and Love<sup>20</sup>, the space group number is according to the International Tables<sup>21</sup>, and the OP direction is that of Stokes and Hatch<sup>16</sup>.

Specifically, N and H refer to the high symmetry points in the bcc Brillouin zone, namely the face center and corner, respectively. Note that a phonon anomaly has been observed at the N-point in the phonon dispersion curves of Ti, Zr and Hf<sup>13,14,15</sup>. It is conceivable that the H-point mechanism may be related to the small anomaly seen at the H-point phonon dispersion of Mg<sup>22</sup>. The crux of the problem is to couple the pathway information to the relevant physics in order to identify which are the most energetically favorable paths.

We generalized the above algorithmic procedure by allowing multiple primary order parameter mechanisms and considering additional user input for some important parameters such as allowed strain, nearest-neighbor distances, and unit-cell size change. This computer program is called COMSUBS and filters possible subgroups through user defined conditions. The program was first used in the description of the rock-salt to CsCl structural change in sodium chloride<sup>23</sup>. We applied the COMSUBS algorithm to the description of the transition of interest here, the hcp to bcc transition in titanium.

For the low-temperature hcp structure,  $G_1 = P6_3/mmc$  with lattice parameter  $a_1 = 2.645 \text{ \AA}$ ,  $c_1 = 4.11 \text{ \AA}$ . For the high-temperature bcc structure,  $G_2 = Im\bar{3}m$  with lattice parameter  $a_2 = 2.91 \text{ \AA}$ . We used the following criteria:

(1) We considered only those subgroups where the length of the lattice generators is  $5.03 \text{ \AA}$  or less. This condition effectively limits the size of the unit cell in the common subgroup, which in turn limits the size of the allowed unit cell parameters.

(2) We considered only those subgroups where the principal elements of the strain tensor are less than  $1 + \epsilon$  and greater than  $(1 + \epsilon)^{-1}$ , where  $\epsilon = 0.5$ . This condition limits the strain (lattice vector lengths) to be within this allowance and also the angle relationships between the group and its subgroup.

(3) The nearest-neighbor distance is  $2.56 \text{ \AA}$  in  $G_1$  and  $2.52 \text{ \AA}$  in  $G_2$ . We considered only subgroups where the nearest-neighbor distance in the structure halfway between  $G_1$  and  $G_2$  is greater than  $2.03 \text{ \AA}$  (80% of the average of  $2.56 \text{ \AA}$  and  $2.52 \text{ \AA}$ ). If the nearest neighbor distance is less than our chosen distance of  $2.03 \text{ \AA}$  we reject the path. Along a rejected path the lattice would need to expand to allow atoms to pass one another and we assume such a strain implies an energy barrier unfavorable to this path.

(4) We considered only maximal subgroups. These define the possible mappings of atoms in  $G_1$  onto atoms in  $G_2$ . Subgroups of these maximal subgroups do not introduce new mappings. They only alter the path by allowing additional distortions in  $G$  along the path.



We check for these additional distortions when a maximal subgroup is selected.

The criteria given above were chosen somewhat subjectively. Each of the criteria could be relaxed and the list would thus be extended. We will see below that the values we chose resulted a list which contained a subgroup that upon initial screening and additional checks for stability is the likely candidate for the pathway mechanism.

Using these criteria, we obtained six subgroups from COMSUBS, which we list in Table III. For the first two entries in the table there is no change in the size of the primitive unit cell relative to the hcp cell. The next two entries are subgroups where the size of the primitive unit cell is doubled. The last two entries are subgroups where the size of the primitive unit cell is three times larger than that of the hcp cell. Subgroups with larger primitive unit cells were not found since we limited the length of the generators according to criterion (1) above. We label the six potential mechanisms we obtained as, (a) ort63A, (b) ort63B, two pathways via orthorhombic space-group 63, (c) mon14, a pathway via the monoclinic space-group 14, (d) mon15, via the monoclinic space-group 15, (e) mon9, via the monoclinic space-group 9, and (f) tri2, via the triclinic space-group 2.

The list obtained by COMSUBS does contain groups in common with those obtained from the four-step algorithm described earlier (for example ort63B), some are excluded by COMSUBS since they do not meet the criteria listed above, and new pathways are obtained due to the allowance of coupled parameters (for example mon14 couples  $N_4^-$  and  $N_2^-$ ).

Prescreening calculations showed (see Table III) that the second pathway based on the orthorhombic space-group Cmcm(63) had the lowest energy barrier among all these paths, and it was chosen for detailed study. The calculations were done at midpoint structures as determined by the bcc-hcp endpoint structures. This distortional mechanism is described in terms of an appropriate high-symmetry point (N) of the bcc Brillouin zone and irreducible representation  $N_4^-$ , with alternating shuffles in the  $\pm[0\bar{1}1]$  directions in the (011) planes. This mechanism is closely related to the original Burgers mechanism.

#### IV. MECHANISMS FOR THE BCC-HCP TRANSFORMATION IN TITANIUM

The most favored transformation path should have the lowest energy among all the paths considered here. Energy of the different paths were computed using an all-electron, full potential linear augmented-plane-wave (FLAPW) method<sup>24</sup>. Calculations were per-

formed scalar-relativistically, neglecting spin-orbit coupling for the valence electrons. Local orbitals<sup>25</sup> were added to enhance the variational freedom and allow the semi-core 3s and 3p orbitals to be treated along with the valence electrons. The added energy parameter was used to simultaneously treat the residual *s* and *p* character of the valence electrons. Our results are insensitive to small changes in all energy parameters.

Our calculations used the generalized gradient approximation (GGA) of Perdew, Burke, and Ernzerhof<sup>26</sup> for the exchange-correlation functional. A muffin-tin sphere with a radius  $R_{\text{MT}}$  was used to define the augmented plane-wave basis functions. No restriction is made as to the shape of the potential or charge density. The size of the FLAPW basis was determined by a plane-wave cutoff,  $K_{\text{max}}$ . The  $K_{\text{max}}$  value is given by the relation  $R_{\text{MT}}K_{\text{max}} = 9.0$ , and was found to be adequate in determining the system energy. 405 irreducible points in the first Brillouin zone of orthorhombic Ti were sampled according to the improved tetrahedron method<sup>27</sup> for Brillouin zone (BZ) integrations. Total energies changed by less than 0.014 eV/atom on increasing the number of BZ points sampled. All self-consistent calculations were iterated until the total energy changed by less than 0.1 meV/atom.

Based on the FLAPW calculations, we found that an intermediate orthorhombic pathway becomes more stable than either of the bcc or hcp end-points for volumes between 49.197 and 50.235 Å<sup>3</sup>. The intermediate orthorhombic phase gives rise to orthorhombic-bcc and hcp-orthorhombic transitions at 61.8 and 51.3 GPa, respectively (See Fig. 2). Because the orthorhombic unit cell and the atoms within it were relaxed to find the lowest energy, these parameters change slightly in this range. In Table IV, we list the relevant atomic and unit cell coordinates near the middle of the stable orthorhombic region. The *y* coordinate refers to the value of *y* in the specification of the Wyckoff *c* position of the form 0, *y*, 1/4. If we ignore this orthorhombic intermediate phase, we find that the bcc-hcp transition occurs at a constant pressure of  $\sim 57$  GPa. The transition pressures were determined by the slope of the common tangent to the energy versus volume curves of the two appropriate phases participating in the transformation. Since the curves are very close to each other in energy, we are unable to determine from the common tangent construction whether the orthorhombic phase is more stable than a mixture of bcc and hcp crystals. We do see that there are regions wherein the orthorhombic system has lower energy than either the hcp or bcc phases.

Since our preliminary calculations pointed to a mechanism operating via a common or-

thorhombic subgroup, we chose to investigate it in more detail. The orthorhombic cells were fully relaxed with respect to its lattice parameters and internal coordinates, a total of four variational parameters, to determine minimum energy configurations. Such minimum energy surfaces for the common orthorhombic subgroup were determined at five different volumes, 49.316, 49.434, 49.716, 50.054, and 50.235  $\text{\AA}^3$ , in the transformation region. We find that the energy of the orthorhombic phase is also sensitive to its lattice constant along the  $c$ -axis. All of the five volumes possessed minimum energy when the orthorhombic cell had a length between 4.04 and 4.07  $\text{\AA}$ . This  $c$ -axis value is significantly different from the value of 4.11  $\text{\AA}$  corresponding to the clamped orthorhombic structure of the hcp phase. Such a variation in the  $c$ -axis lattice constant was not considered in the original Burgers mechanism. The energy versus volume plot for the bcc, hcp and orthorhombic phases in the vicinity of the transformation region is given in Fig. 2. We can see that there is no effective energy barrier to the bcc-hcp transformation when the transformation proceeds via the orthorhombic phase.

## V. DETERMINING FREE-ENERGY FUNCTIONAL FROM FIRST-PRINCIPLES DATA

Here we demonstrate that it is possible to rigorously fit the Ginzburg-Landau free-energy functional to first-principles energy data. These functionals will be used in our future work. One primary and three secondary order parameters (OP's) completely describe the bcc-hcp transition through the orthorhombic phase. They are the intracell atom “shuffle” ( $\eta_1$ ), the shear ( $\eta_2$ ), deviatoric ( $\eta_3$ ), and volumetric ( $\eta_4$ ) strains. Shuffle is the primary OP and is in units of Bohr. The orthorhombic  $c$ -axis parameter gives us a measure of  $\eta_2$ , and is also in the units of Bohr. The deviatoric OP  $\eta_3$ , defined as the ratio of  $a$ - to  $b$ -axis parameters of the orthorhombic cell, is dimensionless. The volumetric OP ( $\eta_4$ ) has the units of Bohr<sup>3</sup>. The full form of the Ginzburg-Landau free-energy functional, involving all four OP's, is given by the equations:

$$\begin{aligned}
 F_L(\eta_1, \eta_2, \eta_3, \eta_4) = & A_1\eta_1^2 + A_2\eta_1^4 + A_3\eta_1^6 \\
 & + A_4\eta_1^2\eta_2^2 + A_5\eta_2^2 + A_6\eta_2^4 \\
 & + A_7\eta_1^2\eta_3^2 + A_8\eta_1^2\eta_2 + A_9\eta_3^2
 \end{aligned}$$

$$\begin{aligned}
& +A_{10}\eta_3^4 + A_{11}\eta_1^2\eta_3 + A_{12}\eta_4^2 \\
& +A_{13}\eta_4^3 + A_{14}\eta_2^2\eta_3 + A_{15}\eta_3^3 \\
& +A_{16}\eta_1^2\eta_4 + A_{17}\eta_2^2\eta_4 + A_{18}\eta_3^2\eta_4,
\end{aligned} \tag{1}$$

$$F_G(\eta_1) = g_1\eta_{1,x}^2 + g_2(\eta_{1,y}^2 + \eta_{1,z}^2) + g_3\eta_{1,y}\eta_{1,z}. \tag{2}$$

Equation (1) is the Landau portion of the free energy and gives the energy for a homogeneous phase arising from coupled primary and secondary OP contributions. Equation (2) contains the (nonlocal gradient) Ginzburg portion of the free energy and gives the energy of heterogeneous solutions, e.g., energies of domain walls configurations, etc. The notation in Equation (2) indicates derivatives of the OP components, e.g.,  $\eta_{1,x}$  is the  $x$  derivative of  $\eta_1$ .

It is important to note that this free-energy is at  $T = 0$  K. The coefficients of  $F_L$ , the Landau portion of the free energy given above, were determined by a Powell non-linear least square fitting<sup>28</sup> of the first-principles energy data, along the bcc-hcp transition path. Since the purpose of this work is to demonstrate the feasibility of fitting GL free-energy functional to first-principles energy data, we carried out the fit at one fixed volume (50.054 Å<sup>3</sup>) falling within the transformational volume region and using 58 energy values corresponding to this volume obtained from first-principles calculation. The coefficients are given in Table V. The fitted energy values had an error of less than 0.5 %. Here, the summation index  $i$  is over all the 58 energy values.

## VI. RESULTS, DISCUSSION AND CONCLUSION

As introduced earlier, Burgers<sup>6</sup> originally derived the orientational relationship between the bcc and hcp phases for the bcc-hcp transformation. This orientational relationship was translated into a mechanism<sup>13,14,15</sup> with three parameters: (a) shuffle of the atoms in the  $\{110\}_{\text{bcc}}$  planes in the  $\langle 1\bar{1}0 \rangle$  directions; a displacement amplitude of  $\frac{\sqrt{2}}{12}$  times the bcc lattice constant leads to the exact hcp stacking sequence, (b) a shear such as  $(1\bar{1}2)[\bar{1}11]$  and  $(\bar{1}12)[1\bar{1}1]$  to squeeze the bcc octahedron to transform it into a regular hcp one; this changes the angle of the hcp face in the basal plane from 70.53° to 60°, and (c) an appropriate volume dilatation to reach the correct end volume. Such a mechanism is similar to our pathway via

the intermediate orthorhombic subgroup in the above three respects. However, our pathway has an additional characteristic in that it also allows the orthorhombic lattice constant along the c-axis to vary. In retrospect, although such a variation is intuitive, it is surprising that Burgers apparently did not factor such a possibility into his mechanism. We suggest that the material should follow our more general four parameter pathway during the transformation. In essence, the utility of our coupled symmetry and first-principles calculations is demonstrated in that we find a Burgers like mechanism, albeit a more generalized one. We used a general and robust algorithm to ferret out the correct mechanism, one that is consistent with the symmetry and physics of the transformation. There is no energy barrier for this new generalized Burgers mechanism.

We have carried out our calculations for  $T = 0$  which may be more accurate for pressure induced transitions such as  $hcp \rightarrow \omega$  in titanium. However,  $bcc \rightarrow hcp$  is a thermal transformation which takes place around 1150 K. Therefore, realistically finite temperature phonon effects<sup>29</sup> cannot be overlooked. We, however, calculated the energies of various frozen phonon structures (using the computer program FROZSL-INIT by L.L. Boyer and H. T. Stokes) that deviate from our calculated orthorhombic pathway and list the relative energies of these distorted structures with respect to the reference orthorhombic energy in Table VI. It is clear that the energy of these phonon distorted structures are higher than that of our orthorhombic pathway. Thus, we expect the overall transformation path to remain Burgers-like at finite temperature except that energy barriers for competing paths may change ( $\sim 100$  meV for this temperature). Work is underway to add the effects of entropy in the free-energy. In addition, defects are invariably present during many phase transformations. Depending on the defect energetics and concentration they may alter the transformation path or in some cases arrest it altogether (e.g. a few ppm oxygen arrests the shock-induced  $hcp \rightarrow \omega$  transformation in titanium). For low energy and low concentration of defects we do not expect our results to change significantly. However, there is a need for systematic evaluation of how defects affect transformation paths and barriers.

To our knowledge this is the first systematic attempt to enumerate transformation paths based on symmetry and then to integrate this information with first principles calculations for the bcc to hcp transformation. Our approach is general and mathematically rigorous with no *ad hoc* or empirical elements involved. We believe that the unique combination of symmetry and electronic structure is an equally powerful tool to identify transforma-

tion mechanisms in many other reconstructive transformations in nature, e.g., the Bain mechanism for fcc to bcc transformation<sup>5</sup>, the Wentzcovitch-Lam mechanism for fcc to hcp transformation<sup>8</sup>, and the diamond to NaCl structure. As we have seen for Ti, this approach also has the possibility of predicting new, unforeseen phases that would be difficult to find by *ad-hoc* guesses. Finally, in addition to a Burgers-like mechanism we predicted new mechanisms,  $N_2^-$  and  $H_4$ , which may well exist in other elements and alloys including Mg.

This research is supported by the Department of Energy under contract W-7405-ENG-36; it used resources of the National Energy Research Scientific Computing Center, which is supported by the Office of Science of the U.S. Department of Energy under Contract No. DE-AC03-76SF00098.

---

\* Present Address: Materials Science Division, Los Alamos National Laboratory, Los Alamos, New Mexico 87545 (sgsrini@lanl.gov).

† Permanent Address: Department of Physics and Astronomy, Brigham Young University, Provo, Utah 84602 (hatchd@byu.edu).

‡ Permanent Address: Department of Physics and Astronomy, Brigham Young University, Provo, Utah 84602.

<sup>1</sup> D.A. Young, *Phase Diagrams of the Elements* (University of California Press, Berkeley, 1976).

<sup>2</sup> J. W. Christian, *Theory of Transformations in Metals and Alloys* (Pergamon Press, Oxford, 1965).

<sup>3</sup> R. E. Reed-Hill and R. Abbaschian, *Physical Metallurgy Principles* (PWS Publishing Co., Boston, 1994).

<sup>4</sup> C. M. Wayman, *Introduction to the Crystallography of Martensitic Transformations* (Macmillan Co., 1964).

<sup>5</sup> E.C. Bain, *Trans. AIME* **70**, 25 (1924).

<sup>6</sup> W. G. Burgers, *Physica* **1**, 561 (1934).

<sup>7</sup> H.E. Cook, *Acta Metall.* **21** 1445 (1973).

<sup>8</sup> R.M. Wentzcovitch and P.K. Lam, *Phy. Rev. B* **44**, 9155 (1991).

<sup>9</sup> J.M. Silcock, *Acta Metall.* **6**, 48 (1958).

- <sup>10</sup> V. P. Dmitriev, Yu. M. Gufan and P. Toledano, *Phy. Rev. B* **44**, 7248 (1991); P. Toledano and V. P. Dmitriev, *Reconstructive Phase Transitions In Crystals and Quasicrystals* (World Scientific, Singapore, 1996).
- <sup>11</sup> P. A. Lindgard and O. G. Mouritsen, *Phy. Rev. Lett.* **57**, 2458 (1986); P. A. Lindgard, *J. de Phys. III* **1**, C4-3 (1991).
- <sup>12</sup> M. Sanati, A. Saxena, T. Lookman, and R. C. Albers, *Phys. Rev B* **63**, 224114 (2001) ; M. Sanati, A. Saxena, and T. Lookman, *Phys. Rev B* **64**, 092101 (2001).
- <sup>13</sup> W. Petry, A. Heiming, J. Trampenau, M. Alba, C. Herzig, H. R. Schober, and G. Vogl, *Phys. Rev. B* **43**, 10933 (1991).
- <sup>14</sup> A. Heiming, W. Petry, J. Trampenau, M. Alba, C. Herzig, H. R. Schober, and G. Vogl, *Phys. Rev. B* **43**, 10948 (1991).
- <sup>15</sup> J. Trampenau, A. Heiming, W. Petry, M. Alba, C. Herzig, W. Miekeley, and H. R. Schrober, *Phys. Rev. B* **43**, 10963 (1991).
- <sup>16</sup> H. T. Stokes and D. M. Hatch, *Isotropy Subgroups of the 230 Crystallographic Space Groups* (World Scientific, Singapore, 1988).
- <sup>17</sup> Y.K. Vohra and P.T. Spencer, *Phys. Rev. Lett.* **86**, 3068 (2001).
- <sup>18</sup> Y. Akahama, H. Kawamura, and T. Le Bihan, *Phys. Rev. Lett.* **87**, 275503 (2001).
- <sup>19</sup> D. M. Hatch, T. Lookman, A. Saxena, H. T. Stokes, *Phys. Rev. B* **64**, 060104 (2001).
- <sup>20</sup> S. C. Miller and W. F. Love, *Tables of Irreducible Representations of Space Groups and Co-Representations of Magnetic Space Groups* (Pruett, Boulder, 1967).
- <sup>21</sup> T. Hahn, Ed., *International Tables for Crystallography, Volume A* (Reidel Publishing Co., Boston, 1983).
- <sup>22</sup> J.D. Althoff, P.B. Allen, R.M. Wentzcovitch, and J.A. Moriarty, *Phys. Rev. B* **48**, 13 253 (1993).
- <sup>23</sup> H. T Stokes, and D. M. Hatch, *Phys. Rev. B* **65**, 144114 (2002).
- <sup>24</sup> P. Blaha, K. Schwarz, and J. Luitz, *WIEN97, A Full Potential Linearized Augmented Plane Wave Package for Calculating Crystal Properties*, (Techn. Universität Wien, Austria, 1999).
- <sup>25</sup> D. J. Singh, *Planewaves, Pseudopotentials and the LAPW Method*, (Kluwer, Boston, 1994).
- <sup>26</sup> J. P. Perdew, K. Burke, and M. Ernzerhof, *Phys. Rev. Lett.* **77**, 3865 (1996).
- <sup>27</sup> P. E. Blöchl, O. Jepsen, and O. K. Andersen, *Phys. Rev. B* **49**, 16223 (1994).
- <sup>28</sup> W.H. Press, B.P. Flannery, S.A. Teukolsky, and W.T. Vetterling, *Numerical Recipes in C The Art of Scientific Computing* (Cambridge University Press, Cambridge, 1988).

<sup>29</sup> S. Rudin, C. Greeff, M.D. Jones, and R.C. Albers, *Phys. Rev. B* **65**,235114 (2002).



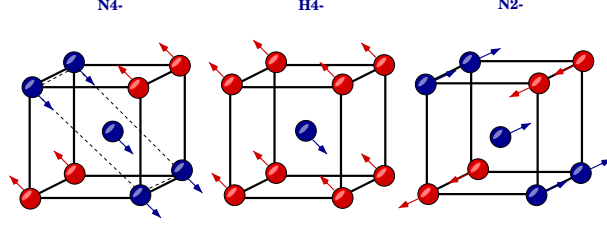


FIG. 1: Three simplest mechanisms that take a bcc phase into a hcp structure, and based on a common orthorhombic subgroup (Space-Group 63,  $Cmcm$ ): (a)  $N_4^-$ , (b)  $H_4^-$ , and (c)  $N_2^-$ .

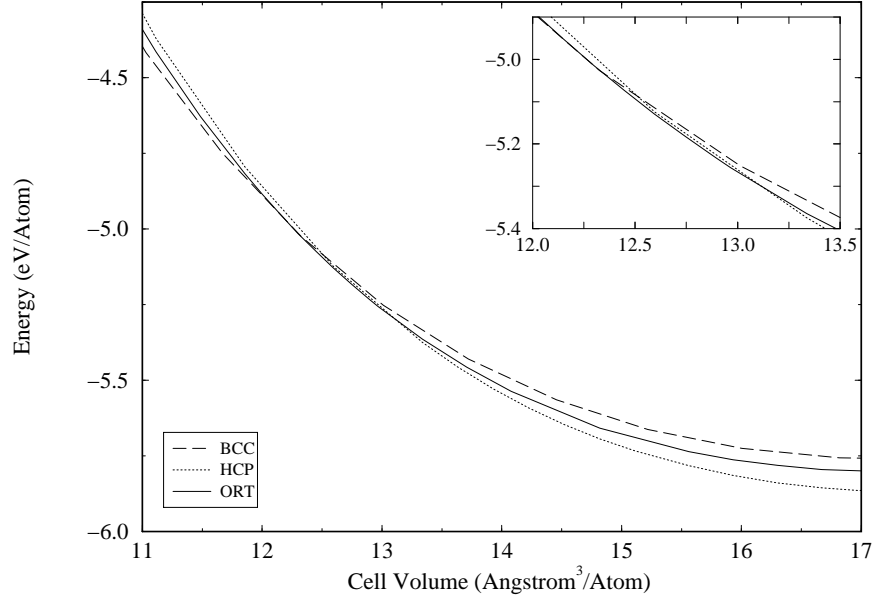


FIG. 2: Energy versus cell volume for the bcc, hcp and orthorhombic phases of titanium. The orthorhombic phase has the lowest energy within the transformation volume region.

TABLE I: Reconstructive transformation mechanisms from the literature.

| Transformation | Mechanism                     |
|----------------|-------------------------------|
| bcc-fcc        | Bain <sup>5</sup>             |
| bcc-hcp        | Burgers <sup>6</sup>          |
| bcc- $\omega$  | Cook <sup>7</sup>             |
| fcc-hcp        | Wentzcovitch-Lam <sup>8</sup> |
| hcp- $\omega$  | Silcock <sup>9</sup>          |

TABLE II: List of all 58 possible mechanisms for the bcc-hcp transformation allowed by symmetry. For each IR, we specify the common subgroup, OP direction, and cell size change. The notation for order parameter direction is that of Stokes and Hatch<sup>16</sup>.

| IR      | Subgroup (OP direction, Cell Size Change)                                                                                                                                            |
|---------|--------------------------------------------------------------------------------------------------------------------------------------------------------------------------------------|
| $H_4^-$ | 11 (C1,2), 63 (P2,2)                                                                                                                                                                 |
| $N_2^-$ | 1 (S4,4), 1 (6D1,8), 2 (C2,4), 2 (S3,8), 2(4D1, 8)<br>5 (S12,8), 5 (4D3,8), 8 (4D6,8), 9 (S13,8), 9(4D4, 8)<br>12 (C8,8), 15 (S6,8), 42 (S14,8), 43 (C19,8),<br>59 (C1,4), 63 (P1,2) |
| $N_3^-$ | 1 (S3,4), 1 (6D1,8), 2 (C2,4), 2 (S4,8), 2 (4D1,8)<br>5 (C8,4), 5 (S12,8), 5 (4D3,8), 5 (4D6,8), 8 (S13,8)<br>8 (4D4,8), 12 (C9,8), 12 (S6,8), 42 (C19,8)                            |
| $N_4^-$ | 1 (S4,4), 1 (6D1,8), 2 (C2,4), 2 (S3,8), 2 (4D1,8)<br>5 (S12,8), 5 (4D3,8), 8 (S13,8), 8 (4D4,8) 9 (4D6,8)<br>12 (S6,8), 15 (C8,8), 42 (C19,8), 43 (S14,8),<br>58 (C1,4), 63 (P1,2)  |
| $P4$    | 1 (6D,4), 2 (S3,4), 5 (S12,4), 5 (S18,4), 5 (4D1,4)<br>8 (4D6,4), 9 (S5,4), 12 (C8,4), 15 (C2,4), 44 (C22,4)                                                                         |

TABLE III: Energies from initial pre-screening calculations for six mechanisms given by the COM-SUBS algorithm. Calculations were done at midpoint structures as determined by the bcc-hcp endpoint structures. Energy is in eV/atom, and the lattice-parameters are in Å. † denotes an unrelaxed energy value. All of the rest are relaxed energy values.

| Mehanism         | Lattice-Constants   | Cell-Angles      | Energy             |
|------------------|---------------------|------------------|--------------------|
| ort63A Cmcm      | (2.78, 4.35, 4.11)  | (90, 90, 90)     | -4.51              |
| ort63B Cmcm      | (2.78, 4.35, 4.11)  | (90, 90, 90)     | -5.05              |
| mon14 P21/c      | (2.57, 4.33, 4.95)  | (90, 116.1, 90)  | -4.84              |
| tri2 P $\bar{1}$ | (4.77, 4.63, 2.54)  | (85, 87.2, 62.5) | -4.43              |
| mon9 Cc          | (10.25, 4.32, 4.47) | (90, 48.7, 90)   | -4.70 <sup>†</sup> |
| mon15 C2/c       | (8.18, 4.27, 5.90)  | (90, 46.2, 90)   | -4.24              |

TABLE IV: Sample atomic and unit cell coordinates for the intermediate orthorhombic phase. The unit cell parameters are in Å, the cell angles are in degrees, and the  $y$  coordinate is in fractional atomic units. The  $y$  coordinate refers to the value of  $y$  in the specification of the Wyckoff  $c$  position of the form  $0, y, 1/4$ .

| Space-Group | Lattice-Constants  | Cell-Angles  | $y$ coordinate |
|-------------|--------------------|--------------|----------------|
| 63 Cmc      | (2.92, 4.29, 4.02) | (90, 90, 90) | 0.295          |

TABLE V: Ginzburg-Landau free-energy coefficients in Eq. 1 for the bcc-hcp transformation in Ti via the  $N_4^-$  mechanism.  $F_L$  is in eV,  $\eta_1$  and  $\eta_2$  are in Å,  $\eta_3$  is dimensionless, and  $\eta_4$  is in Å<sup>3</sup>.

|                      |                     |                      |
|----------------------|---------------------|----------------------|
| $A_1 = -48106.70$    | $A_2 = +319.26$     | $A_3 = +1412.71$     |
| $A_4 = -312.31$      | $A_5 = -848.33$     | $A_6 = +6.94$        |
| $A_7 = +26707.92$    | $A_8 = +7434.47$    | $A_9 = -44094.63$    |
| $A_{10} = -19221.73$ | $A_{11} = -2145.13$ | $A_{12} = +0.00$     |
| $A_{13} = +0.00$     | $A_{14} = -565.07$  | $A_{15} = +27635.83$ |
| $A_{16} = +0.00$     | $A_{17} = +0.00$    | $A_{18} = +0.00$     |

TABLE VI: Relative energy ( $\Delta E$ ), in units of meV/atom, of various frozen-phonon structures that deviate from the transformation pathway via the common orthorhombic subgroup. The energy of the orthorhombic subgroup is used as reference. The cell volume is in  $\text{\AA}^3/\text{atom}$ . Some IR's have *multiple* frozen phonon configurations. Energies of IR's with multiple frozen phonon configurations are listed in the same line.

| IR           | Space-group | $\Delta E$         |
|--------------|-------------|--------------------|
| $\Gamma_1^+$ | 63 $Cmcm$   | 0                  |
| $\Gamma_2^+$ | 11 $P121/m$ | 170                |
| $\Gamma_3^+$ | 12 $C2/m$   | 1775               |
| $Y_1^+$      | 51 $Pmma$   | 792                |
| $Y_2^+$      | 62 $Pnma$   | 9219               |
| $Y_3^+$      | 58 $Pnnm$   | 71                 |
| $Y_2^-$      | 62 $Pnma$   | 639                |
| $Y_3^-$      | 57 $Pmmm$   | 391                |
| $Y_4^-$      | 59 $Pmmn$   | 31                 |
| $Z_1$        | 12 $C2/m$   | 41, 449, 255       |
| $Z_2$        | 15 $C2/c$   | 54                 |
| $S_1^+$      | 11 $P121/m$ | 187, 551, 650, 305 |
| $S_1^-$      | 14 $P21/c$  | 332                |
| $S_2^-$      | 11 $P121/m$ | 347, 483, 612      |
| $T_1$        | 12 $C2/m$   | 738, 622, 364, 238 |